HHS Public Access

Author manuscript

J Bone Miner Res. Author manuscript; available in PMC 2019 June 01.

Published in final edited form as:

J Bone Miner Res. 2018 June ; 33(6): 1114–1125. doi:10.1002/jbmr.3398.

PGC1β Organizes the Osteoclast Cytoskeleton by Mitochondrial Biogenesis and Activation

Yan Zhang[1,2], **Nidhi Rohatgi**[1], **Deborah J. Veis**[1,3], **Joel Schilling**[4], **Steven L. Teitelbaum**[1,3,*], and **Wei Zou**[1,*]

[1]Department of Pathology and Immunology, Washington University School of Medicine, St. Louis, Missouri, 63110

[2]Center for Translational Medicine, The First Affiliated Hospital of Xi'an Jiaotong University, Xi'an, Shanxi 710061, People's Republic of China

[3]Department of Medicine, Division of Bone and Mineral Diseases, Washington University School of Medicine, St. Louis, Missouri, 63110

[4]Department of Medicine, Division of Cardiology, Washington University School of Medicine, St. Louis, Missouri, 63110

Abstract

Osteoclasts are mitochondria-rich cells but the role of these energy-producing organelles in bone resorption is poorly defined. To this end, we conditionally deleted the mitochondria-inducing co-activator, PGC1β, in myeloid lineage cells to generate PGC1β^{LysM} mice. In contrast to previous reports, PGC1β-deficient macrophages differentiate normally into osteoclasts albeit with impaired resorptive function due to cytoskeletal disorganization. Consequently, bone mass of PGC1β^{LysM} mice is double that of WT. Mitochondrial biogenesis and function are diminished in PGC1β^{LysM} osteoclasts. All abnormalities are normalized by PGC1β transduction. Furthermore, OXPHOS inhibitors reproduce the phenotype of PGC1β deletion. PGC1β's organization of the osteoclast cytoskeleton is mediated by expression of GIT1 which also promotes mitochondrial biogenesis. Thus, osteoclast mitochondria regulate the cell's resorptive activity by promoting cytoskeletal organization.

Introduction

Osteoclasts are derived from bone-marrow derived monocyte-macrophages (BMMs) and their differentiation occurs under the aegis of macrophage colony-stimulating factor (M-CSF) and receptor activator of nuclear factor kappa-B ligand (RANKL). When degrading skeletal tissue, osteoclasts adhere to the bone surface and form a "gasket-like" structure, known as the actin ring or sealing zone, to isolate the resorptive microenvironment from the general extracellular space (1)(1). Generation of this isolated microenvironment requires

Contact Information, Wei Zou, PhD., Washington University School of Medicine, Department of Pathology and Immunology, Campus Box 8118, 660 South Euclid Avenue, St. Louis, MO 63110, Phone: (314) 454-8463, Fax: (314) 454-5505, weizou@wustl.edu, Steven L. Teitelbaum, M.D., Washington University School of Medicine, Department of Pathology and Immunology, Campus Box 8118, 660 South Euclid Avenue, St. Louis, MO 63110, Phone: (314) 454-8463, Fax: (314) 454-5505, teitelbs@wustl.edu.

*Co-senior Authors

polarization of the osteoclast's resorptive machinery to the cell/bone interface (2). Therefore, organization of the osteoclast cytoskeleton is an essential component of the cell's capacity to resorb bone.

Peroxisome proliferator-activated receptor gamma coactivators-1 β (PGC1β) is a master regulator of mitochondrial biogenesis and respiration, profusely expressed in tissues of high oxidative metabolism such as brown adipose tissue, heart and skeletal muscle. PGC1β, but not PGC1α, another stimulator of mitochondrial biogenesis, is induced during osteoclast differentiation (3–5). Despite their induction by PGC1β, in osteoclasts, the contribution the cell's abundant mitochondria make to the resorptive process is poorly defined. For example, previous studies reported the co-activator is essential for osteoclast differentiation, an event presumably requiring mitochondrial activity (3, 4). This conclusion is inconsistent, however, with the normal number of osteoclasts in PGC1β−/− mice (3).

To identify the role of PGC1β in osteoclastogenesis, we generated PGC1β conditional knockout mice in which the gene is exclusively deleted in myeloid lineage cells by Lysozyme M (Lys M) Cre ($PGC1\beta^{LysM}$). Challenging previous reports, we find osteoclast differentiation of PGC1β-deficient BMMs is unaltered in vitro and in vivo. However, osteoclast function is impaired when PGC1β is deleted and is attended by cytoskeletal dysfunction. Because of compromised bone resorption, $PGC1\beta^{LysM}$ mice are osteopetrotic. Rac1 and c-Src activation are unaltered in $PGC1\beta^{LysM}$ osteoclasts establishing a non-canonical mechanism generates their abnormal cytoskeleton. On the other hand, mitochondrial biogenesis and energy expenditure are substantially diminished in the mutant cells likely mediated by reduced expression of GPCR Kinase 2 interacting protein1 (GIT1). Furthermore, mitochondrial respiratory inhibitors suppress actin ring formation and mimic the PGC1β knockout phenotype whereas enhancement of mitochondrial biogenesis with PGC1α overexpression normalizes PGC1β-deficient osteoclasts. These observations establish, for the first time, that the bone resorptive capacity of individual osteoclasts is enabled by mitochondria-mediated cytoskeletal organization.

Results

PGC1β regulates osteoclast function but not differentiation

To determine the role of PGC1β in osteoclastogenesis, we generated conditional knockout mice in which the gene is exclusively deleted in myeloid lineage cells ($PGC1\beta^{LysM}$) (Supp Fig 1A). $PGC1\beta^{LysM}$ or Cre- (WT) bone marrow macrophages (BMMs) were cultured with M-CSF and RANKL to promote osteoclastogenesis. Indicating PGC1β does not retard formation of the bone resorptive cell, immunoblots of osteoclast differentiation markers, NFATc1, cathepsin K, and integrin β3 are indistinguishable in WT and PGC1β-deficient cells (Fig 1A). The same holds regarding TRAP5b, a marker of osteoclast tissue abundance (Fig 1B). While NFATc1 and cathepsin K mRNAs mirror protein expression, for reasons unknown, β3 integrin mRNA is substantially greater than control (Fig 1C). Confirming unaltered differentiation of $PGC1\beta^{LysM}$ cells, the proportions of culture wells occupied by mutant and WT osteoclasts, defined as TRAP-expressing cells containing at least 3 nuclei, are similar (Fig 1D).

Having established PGC1β does not regulate osteoclast differentiation, in vitro, we turned to osteoclast function, namely the capacity of the individual resorptive cell to degrade bone. To this end we cultured equal numbers of WT or mutant BMMs on bone slices and after 6 days measured resorptive pit formation. Whereas WT osteoclasts resorb approximately 60% of bone surface, pits are essentially absent in cultures containing PGC1β-deficient cells (Fig 1E, Supp Fig 1B). Confirming PGC1β-deletion in osteoclast lineage cells arrests bone resorption, medium CTx (c-terminal telopeptides type I collagen), a marker of bone matrix degradation, is significantly reduced in mutant cultures (Fig 1F). The difference in relative magnitude of in vitro and in vivo data may represent assay precision. Thus, PGC1β regulates osteoclast function but not formation, in vitro.

We next asked if the same occurs in vivo. In fact, osteoclast abundance and serum TRAP5b are normal, in PGC1β^{LysM} mice (Fig 2A,B). While x-Ray and μCT reveal a significant increase in bone mass, osteogenesis is unchanged as documented by unaltered serum osteocalcin and P1NP (procollagen type I N-terminal propeptide) (Fig 2C,D, Supp 2B–D). Thus, PGC1β modulates osteoclast function but not differentiation or abundance.

PGC1β organizes the osteoclast cytoskeleton in a non-canonical manner

While PGC1β^{LysM} osteoclasts are normal in abundance, they are morphologically distinct. Mutant BMMs, exposed to at least 50 ng/ml RANKL, differentiate into osteoclasts which are substantially larger and contain more nuclei than WT (Fig 3A,B, Supp 3A). Like their in vitro counterparts, PGC1β^{LysM} osteoclasts, in vivo, are approximately 4 fold larger and more spherical than WT (Fig 3C,D). Furthermore, the % of PGC1β^{LysM} osteoclast surface juxtaposed to bone, in PGC1β^{LysM} mice, is significantly reduced (Fig 3E).

The size of PGC1β^{LysM} osteoclasts and their compromised capacity to attach to bone suggests abnormal cytoskeletal function. In keeping with dysfunctional cytoskeletal organization, PGC1β^{LysM} osteoclasts are essentially incapable of forming actin rings (Fig 4A). Confirming PGC1β's cytoskeletal organizing properties, its retroviral transduction into mutant BMMs completely rescues actin ring formation by differentiated cells and reduces their size to that approximating WT (Fig 4B,C, Supp Fig 3B).

Actin ring formation requires organization of globular actin (G-actin) into its fibrillar state (F-actin) (6). To explore this issue in the context of PGC1β^{LysM} deficiency, conditionally deleted and WT osteoclasts, generated on bone, were starved and recultured in medium with or without M-CSF which organizes the cell's cytoskeleton. As expected, M-CSF generates F-actin. In keeping with their compromised capacity to form actin rings and resorb bone, the abundance of F-actin in PGC1β^{LysM} osteoclasts is substantially less than in their WT counterparts regardless of the presence of M-CSF (Fig 4D).

Presence of the ruffled border, which is the osteoclast resorptive organelle, also depends on cytoskeletal organization as it is formed by transport of intracellular vesicles to the bone-apposed plasma membrane with which it fuses under the aegis of molecules such as synaptotagmin VII (2). Consistent with a dysfunctional cytoskeleton, PGC1β^{LysM} osteoclasts lack ruffled borders and evidence of associated pit formation (Fig 4E). Unexpectedly in face of increased cell size, expression of proteins known to promote fusion

of osteoclasts including CD47, SIRPα, V-ATPase VO D2 and DC-Stamp are not increased in PGC1β^{LysM} BMMs and mature polykaryons (Supp Fig 3C).

Integrin- (outside-in) (7) and cytokine- (inside-out) (8, 9) osteoclast cytoskeletal organization is mediated by canonical signaling of which activated c-Src and Rac1 are critical components. Deletion of c-Src, Rac1 or any of the intermediary signaling molecules arrests organization of the cytoskeleton but results in a phenotype distinct from that of cells lacking PGC1β in that the former do not “superspread” but are contracted with a “crenated” appearance (10). This distinction suggested that the signaling pathway mediating c-src/Rac1cytoskeletal organization may differ from that induced by PGC1β. To determine if the cytoskeletal disorganization attending PGC1β-deletion reflects arrest of the canonical pathway, we assessed the activation state of c-Src and Rac upon integrin or cytokine stimulation.αvβ3, the principal c-Src/Rac1 cytoskeleton-organizing integrin in osteoclasts, is activated by the RGD motif present in vitronectin. We thus plated pre-fusion osteoclasts on vitronectin-coated or non-coated plates (Supp Fig 3D). As expected, αvβ3 stimulation activated c-Src as manifest by S416 phosphorylation and Rac1 by GTP association in WT pre-osteoclasts. The same, however, occurred in PGC1β^{LysM} pre-osteoclasts. Similarly, inside-out stimulation by M-CSF yielded no difference in c-Src or Rac1 activation in WT and mutant cells (Supp Fig 3E). Thus, absence of PGC1β compromises the osteoclast cytoskeleton in a manner other than disruption of the canonical signaling pathway.

PGC1β promotes mitochondrial biogenesis and activation in mature osteoclasts

PGC1β regulates mitochondrial biogenesis in osteoclasts (3, 4). In contrast to our findings, however, this observation was made in cells in which PGC1β is reported to arrest formation of the polykaryon and not its function. To determine if the same holds in the context of arrested cytoskeletal organization, we examined mitochondrial biogenesis in PGC1β^{LysM} osteoclasts and their BMM precursors. In keeping with the robust acquisition of mitochondria as precursors differentiate into mature bone resorptive polykaryons, each mitochondrial marker gene is much less abundant in BMMs than in osteoclasts (Fig 5A). PGC1β deletion however, substantially reduces Cox1(cytochrome oxidase subunit I), Cox3 (cytochrome oxidase subunit III), Cytb (cytochrome b)and ND4 (NADH dehydrogenase 4) in both BMMS and mature osteoclasts. Four of the 5 established oxidative phosphorylation (OXPHOS) complexes are also much more abundant in osteoclasts than BMMs and markedly diminished, in each, absent PGC1β (Fig 5B). Consistent with these observations, mitochondrial mass, detected by mito-tracker (Supp Fig 4A) staining, as well as mitochondrial number (Fig 5C), are decreased in PGC1β-depleted osteoclasts. Mitochondria residing in PGC1β^{LysM} osteoclasts are also morphologically distinct in that they are elongated and lack the spherical phenotype of their WT counterparts (Fig 5D) (11). In keeping with similar, low mitochondrial abundance, XF Cell Mito Stress (Seahorse) analysis reveals no differences in oxygen consumption rate (OCR) of early WT and PGC1β^{LysM} committed osteoclast precursors (Supp Fig 4B,C). In contrast, basal respiration, ATP - coupled respiration and maximal respiration are greatly reduced in mature osteoclasts lacking PGC1β (Fig 5E). Retroviral-mediated re-expression of PGC1β in the knockout osteoclasts completely rescues their impaired mitochondrial biogenesis (Fig 5F). Finally, the rate of glycolysis (ECAR) increases in PGC1β^{LysM} osteoclasts stimulated with glucose (Fig

5G). Collectively, these results demonstrate that the mitochondrial biogenesis and function, but not glycolytic activity, are dampened in PGC1β^{LysM} osteoclasts.

Mitochondrial OXPHOS regulates osteoclast cytoskeletal organization

With determination that PGC1β^{LysM} osteoclasts are both cytoskeletal and mitochondrial deficient we asked if the two events are related. To this end we first exposed WT osteoclasts to cold PBS which disrupts actin ring formation, an event rescued by 5 hours treatment with RANKL (2) (Supp Fig 5A). We then turned to three mitochondrial complex inhibitors of oxidative phosphorylation. Rotenone blunts the transfer of electrons from complex I to ubiquinone, interfering with NADH during the production of cellular ATP. Antimycin A arrests complex III (cytochrome c reductase) thereby interfering with the Q-cycle of enzyme turn over thus disrupting formation of the proton gradient across the mitochondrial inner membrane and ATP production. Oligomycin inhibits ATP synthase (complex V) by blocking its proton channel (Fo subunit), which is necessary for oxidative phosphorylation of ADP to ATP. Simultaneous addition of any of three mitochondrial complex inhibitors virtually arrests the capacity of RANKL to induce formation of this classical manifestation of osteoclast cytoskeletal organization and function (Fig 6A, Supp Fig 5B). To further assess the role of mitochondrial function in actin ring formation we retrovirally expressed PGC1α, which is absent in osteoclasts but promotes mitochondria formation and function in other cells (3–5). In fact, mitochondrial function, as indicated by the mRNA expression of marker genes and ATP-coupled respiration, is significantly restored in PGC1β^{LysM} osteoclasts by PGC1α (Fig 6B,C). Fortifying the concept of mitochondrial regulation of the osteoclast cytoskeleton, PGC1α is as effective in inducing actin ring formation and normalizing size of PGC1β^{LysM} osteoclasts as is the deleted gene (Fig 6D,E; Supp Fig 5C, D).

Paxillin does not mediate the cytoskeletal effects of PGC1β deficiency

PGC1β contains a number of established regulatory domains including those capable of recognizing DNA or RNA (Supp Fig 6A). Additionally, PGC1β contains host cell factor 1 (HCFC1) binding domains and nuclear receptor-associating LXXLL motifs. Transduction of specific deletion mutants of these various domains into PGC1β^{LysM} establishes that only the DNA binding motif is essential for rescue of cytoskeletal organization as manifest by actin ring formation (Fig 7A,B). This observation suggests the capacity of PGC1β to modulate osteoclast function is likely transcriptionally based and due to induction of a regulatory protein(s) affecting cytoskeletal organization and mitochondria. Based on our previous observations, paxillin presented as a candidate inductive target of PGC1β (12).

Paxillin is critical to osteoclast cytoskeletal organization. Like absence of PGC1β^{LysM}, paxillin deletion results in enlarged, rather than “crenated” osteoclasts. This similarity raised the possibility that the superspread appearance of PGC1β^{LysM} osteoclasts is mediated by paxillin deficiency. The abundance of paxillin is, however, unaltered in PGC1β^{LysM} osteoclasts (Supp Fig 6B). Furthermore, paxillin overexpression does not rescue the impaired mitochondrial biogenesis extant in these cells (Supp Fig 6C). Most importantly, paxillin overexpression does not restore the normal size or actin ring forming capacity of PGC1β^{LysM} cells (Supp Fig 6D).

GIT1 mediates PGC1β-induced cytoskeleton organization

The previous experiments establish paxillin does not mediate the cytoskeletal abnormalities of PGC1β^{LysM} osteoclasts. On the other hand, the similar superspread appearance of osteoclasts deleted of either protein raised the possibility that a paxillin regulating moiety also mediates the cytoskeletal effects of PGC1β.

GIT1 is a scaffold protein expressed in a variety of cells. Cytoskeletal organization is among its most prominent properties which it does by interacting with paxillin (13). In osteoclasts, GIT1 organization of the cytoskeleton involves distribution of podosomes, the organelles which form actin rings (14). Its cytoskeletal effects and the fact that it promotes mitochondrial biogenesis in cardiac tissue, suggested GIT1 may participate in PGC1β's regulation of osteoclast function (15). Fortifying this hypothesis, GIT1 is diminished in PGC1β^{LysM} osteoclasts and normalized by PGC1β^{LysM} transduction (Fig 7C). The giant phenotype of PGC1β^{LysM} osteoclasts and their failure to generate actin rings are significantly rescued by GIT1 overexpression, indicating that GIT1 contributes to the cytoskeletal-organizing properties of PGC1β (Fig 7D,E). Consistent with GIT1 rescuing their cytoskeleton, at least in part, via stimulated mitochondrial biogenesis, expression of WT GIT1significantly enhances expression of the mitochondrial enzymes Cox1, Cox3, ND4 and Cytb by PGC1β^{LysM} osteoclasts (Fig 7F). Thus, PGC1β regulates the osteoclast cytoskeleton and thus the cell's resorptive capacity in a mitochondrial/GIT1-dependent manner.

Discussion

Therapeutic regulation of the osteoclast may occur by altering its abundance or its function, namely the capacity of the individual cell to resorb bone. The former typically involves retarding proliferation of osteoclast precursors and their differentiation into mature resorptive polykaryons and/or promoting apoptosis. Osteoclast function, on the other hand, often reflects cell motility and delivery of bone-degrading molecules into the resorptive microenvironment, both of which require cytoskeletal organization. All presently approved resorption-inhibiting drugs enhance bone mass by reducing osteoclast abundance. While these agents substantially reduce fracture risk, their use is complicated by dampening bone turnover or remodeling. Because remodeling is essential for replacement of effete bone with new, the skeletal quality of patients receiving current anti-osteoclastic drugs may be compromised, predisposing to complications such as atypical femoral fracture.

Bone remodeling involves osteoclast-mediated mobilization of osteoblast-attracting factors, such as TGFβ, from bone matrix. There is, however, substantial evidence that osteoclasts, *per se*, secrete proteins which promote osteogenesis irrespective of their resorptive capacity (16). Clinical evidence indicates that a therapeutic strategy whereby bone resorption is attenuated but osteoclasts are dysfunctional, yet survive, may obviate the problem of suppressed bone formation (17).

In 2009 Ishii et al observed that global absence of PGC1β increased bone mass and compromised mitochondrial biogenesis in osteoclasts (3). Unexpectedly, while PGC1β knockdown arrested osteoclast formation in vitro, the number of bone resorbing cells in vivo

was unaltered although their morphology was abnormal. The authors concluded that PGC1β mediates osteoclast formation but its absence, in vivo, is likely compensated by osteoblast-produced cytokines, particularly RANKL. The increased bone mass in face of normal numbers attending PGC1β deletion was postulated to reflect compromised osteoclast function by mechanisms unknown.

In 2010, Wei et al conditionally deleted PGC1β in myeloid lineage cells using mice expressing Tie2 Cre which also targets endothelial lineage cells (4). They noted that, in contrast to globally deficient mice, Cre+ mice had decreased numbers of bone resorptive cells, in vivo, but no alteration of bone mass. Thus, both studies conclude PGC1β mediates osteoclast formation but its role in osteoclast function remained controversial.

In contrast to the previous studies, we find that absence of PGC1β, exclusively in myeloid lineage cells, does not affect osteoclast differentiation in vitro or in vivo while trabecular bone mass is approximately double that of Cre- counterparts. Given unaltered bone formation, as evidenced by circulating osteocalcin, these data confirm that PGC1β effects bone resorption but does so by arresting osteoclast function and not differentiation. The differences between the present and previous studies regarding PGC1β and osteoclastogenesis are unclear but may reflect dissimilar gene targeting or culture conditions.

Activation of integrins, particularly αvβ3, or exposure to the osteoclastogenic cytokines, RANKL or M-CSF, promotes organization of the osteoclast cytoskeleton and stimulates the cell's resorptive capacity. These stimuli exert their effects via a canonical signaling pathway involving c-Src, Syk, Dap12, Vav 3 and Rac. Absence of any component of this pathway eventuates in a common phenotype in which the osteoclast is contracted ("crenated") and fails to form actin rings or ruffled borders.

We find PGC1β deficiency also obviates actin ring and ruffled border formation but the phenotype of PGC1β^{LysM} osteoclasts differs from those lacking components of the integrin/cytokine activated signaling pathway. In contrast to the contracted appearance of the latter, PGC1β deficiency results in markedly enlarged, superspread osteoclasts which fail to attach to bone, in vivo, or form resorption pits, in vitro.

While there is evidence that mitochondrial function is related to the cytoskeleton this relationship is largely postulated to involve facilitation of mitochondrial energy production by cytoskeletal structures such as beta-tubulin II (18). On the other hand, Miyazaki et al propose that mitochondria-produced ATP negatively effects bone resorption in a paracrine/autocrine manner by disrupting the cytoskeleton (19). These authors conclude that a reciprocal relationship exists between mitochondrial function and the osteoclast's resorptive capacity. We find however, that consistent with robust mitochondrial biogenesis, oxidative phosphorylation and attendant ATP-coupled respiration increase as precursors differentiate into the resorptive polykaryon. Moreover, a diminution in mitochondrial function and ATP coupled respiration attends cytoskeletal dysfunction and arrest of the cell's resorptive properties an event likely reflecting impaired conversion of globular to fibrillar actin. These findings uniquely indicate that, in the osteoclast, oxidative phosphorylation promotes

cytoskeletal organization to facilitate bone degradation. This conclusion is fortified by the capacity of oxidative phosphorylation inhibitors to mirror the actin-ring-arresting effects of PGC1β deletion.

In 2013, Indo et al noted, by mechanisms unknown, that glycolytic activity increases osteoclast function (20). Our findings indicate, however, that glycolysis is unlikely to contribute to the osteoclast-activating properties of PGC1β as ECAR is increased in PGC1β^{LysM} osteoclasts. Furthermore, PGC1α, which promotes mitochondrial biogenesis but suppresses glycolysis, completely rescues the PGC1β^{LysM} osteoclast phenotype (21).

GIT1 is an adaptor protein which delivers signaling proteins to focal adhesions and the leading edge of motile cells (13, 14). The ability of GIT1 to localize to the cell's leading edge and modulate cell motility depends upon its association with paxillin whose deletion results in a phenotype similar to osteoclasts lacking PGC1β. Like PGC1β ^{LysM} mice, the bone mass of those deleted of GIT1 is increased yet osteoclast number is unaltered. Confirming arrested function is due to cytoskeletal disorganization, the resorptive capacity of GIT1−/− osteoclasts is markedly diminished (14). Furthermore actin ring generation is reduced in face of normal c-src activation.

Given the many common features of PGC1β- and GIT1-deficient osteoclasts we explored the relationship between the two proteins. We found GIT1substantially diminished in PGC1β ^{LysM} osteoclasts, a defect corrected by PGC1β transduction. Moreover, GIT1 overexpression rescues the cytoskeletal defects of PGC1β deletion. As noted in cardiac myocytes, GIT1 enhances mitochondrial biogenesis in the mutant osteoclasts (Pang et al., 2011). Whereas the suppressive impact of GIT1 deletion on mitochondrial biogenesis in cardiac myocytes is postulated to reflect reduced abundance of PGC1 proteins, it rescues this process, in osteoclasts, independent of PGC1β expression.

Our observations establish that PGC1β promotes osteoclast function but not formation. It appears that the process represents, at least in part, PGC1β induction of GIT1 which, as in other cells, stimulates mitochondrial biogenesis and promotes podosomal organization. Perhaps the most significant and unique aspect of these observations is the documentation that the process reflects osteoclast cytoskeletal organization mediated by mitochondrial oxidative phosphorylation. Furthermore, the fact that PGC1β or GIT1 deficiency increases skeletal mass by arresting osteoclast function, while maintaining viability, suggests they and other mitochondria-stimulating proteins may be therapeutically targeted to inhibit bone resorption while maintaining formation.

Material and Method

Reagents and Mice

Recombinant murine M-CSF was obtained from R&D Systems (Minneapolis, MN). Glutathione S-transferase (GST)-RANKL was expressed in our laboratory as described (Lam et al., 2000). The source of antibodies and reagents is as follows: NFATc1 (Santa cruz), c-Src, phospho-Src (Ser416), integrin β3 (Cell Signaling), cathepsin K (Invitrogen), OXPHOS cocktail (Abcam), beta-actin (Sigma). Rotenone, oligomycin, antimycin A and all

other chemicals were obtained from Sigma. To generate PGC1βLysM mice, PGC1βflox/flox mice were mated with LysM-Cre mice. Mice were housed in the animal care unit of Washington University School of Medicine, where they were maintained according to guidelines of the Association for Assessment and Accreditation of Laboratory Animal Care. All animal experimentation was approved by the Animal Studies Committee of Washington University School of Medicine. Male and female mice were included.

Macrophage isolation and osteoclast culture

All in vitro experiments were performed at least 3 times. Primary bone marrow macrophages (BMMs) were prepared as described (22) with slight modification. Marrow extracted from femora and tibiae of 6- to 8-wk-old mice were cultured in alpha-Minimum Essential Medium Eagle (α-MEM) containing 10% inactivated fetal bovine serum (FBS), 100 IU/ml penicillin, and 100 μg/ml streptomycin (α-10 medium) with 1:10 CMG condition media on petri-plastic dishes. Cells were incubated at 37°C in 6% CO2 for 3 days and then lifted with 1x trypsin/EDTA in PBS. A total of 5×10^5 BMMs were cultured in 5 ml α-MEM containing 10% FBS with 100 ng/ml GST-RANKL and 30 ng/ml M-CSF in 60mm tissue culture dishes. Otherwise BMMs were induced in 48-well or 96-well tissue culture plates proportionally, some containing sterile bone slices. Osteoclast cultures on plastic were terminated at 5 days and on bone, at 6 days.

Plasmids and Retroviral Transduction

Constructs expressing wild or mutant types of mouse PGC-1β, wild type PGC1α, GIT1 and Paxillian in pMX retroviral vector was transfected into the PlatE cells. The medium was changed on the next day, then was harvested, filtered, and infected the Day 2 BMMs in the presence of 1:10 CMG and 4 μg/ml polybrene (Sigma). Twenty-four hours later, the cells for selected with 1 μg/ml blastocidin at least for 3 days before use as osteoclast precursors.

RNA Extraction and quantitative qPCR

Total RNA was extracted using RNeasy RNA purification kit (Qiagen). Complementary DNA (cDNA) was synthesized from 1 μg of total RNA using the iScript cDNA synthesis kit (Bio-Rad). Quantitative qPCR was performed using the PowerUp SYBR Green Master Mix kit (Applied biosystems) and gene specific primers. PCR reactions for each sample were performed with 7500 fast Real-Time PCR System (Applied Biosystems, Foster City, CA, USA) using the comparative threshold cycle (Ct) method for relative quantification. The glyceraldehyde-3-phosphate dehydrogenase (GAPDH) gene was used as an endogenous control. The sequences of primers can be provided upon request.

Western blotting

Cells were harvested and lysed in radioimmunoprecipitation assay (RIPA) buffer containing 20 mM Tris- HCl, pH 7.5, 150 mM NaCl, 1 mM EDTA, 1 mM EGTA, 1% Triton X-100, 2.5 mM sodium pyrophosphate, 1 mM β-glycerophosphate, 1 mM Na3VO4, 1 mM NaF, and 1× protease inhibitor mixture (Roche Applied Science). Protein concentrations were measured using the BCA protein assay (Pierce). The cell lysates were resolved by 10% sodium dodecylsulfate–polyacrylamide gel electrophoresis (SDS-PAGE) and transferred to PVDF

membranes (Amersham Biosciences). After blocking in 0.1% casein in PBS, membranes were incubated with primary antibodies 4°C overnight, followed by incubation with fluorescence-labeled secondary antibodies (Jackson ImmunoResearch Laboratories). Proteins were detected with the Odyssey Infrared Imaging System (LI-COR Biosciences).

Tartrate-resistant acid phosphatase (TRAP) staining assay

Cells were fixed and stained for tartrate-resistant acid phosphatase (TRAP) activity after 5 days in culture, using a commercial kit (Sigma 387-A, St. Louis, MO).

Pit formation assay

After 6 days of culture, bone slices were incubated in 0.5 N NaOH for 30 seconds and cells scraped off using a cotton swab, then incubated with 20 μg/mL peroxidase-conjugated wheat germ agglutinin (Sigma) in PBS for 30 min, washed with PBS three times, and exposed to 3,3′-Diaminobenzidine tablets (Sigma; D4168) for 15 min before washing. BioQuant OSTEO 2010 (BioQuant Image Analysis Corporation, Nashville, TN, USA) was used to quantify pit area.

Histology and histomorphometry

The femurs of 3-month-old mice were fixed with 10% neutral buffered formalin, followed by decalcification in 14% EDTA for 10 days, paraffin embedding, and TRAP staining. Static and dynamic histomorphometric parameters were measured using BioQuant OsteoII (BioQuant Image Analysis Corporation, Nashville, TN) in a blinded fashion. Image J software was used to measure the osteoclast to quantify the area of individual osteoclasts and the % of osteoclast surface juxtaposed to bone.

Microcomputed tomography (μCT)

The trabecular volume of the distal femoral metaphysis was measured using a Scanco μCT40 scanner (Scanco Medical AG, Bassersdorf, Switzerland). A lower threshold of 190 (for female) or 200 (for male) were used for evaluation of all scans. 50 slices were analyzed, starting with the first slice in which condyles and primary spongiosa were no longer visible.

Actin ring formation assay

After 6 days of osteoclastic induction on bone slices, the osteoclasts were fixed and stained with FITC-phalloidin at room temperature for 1 hour to visualize actin rings. In the mitochondrial inhibitor treatment assay, day 6 osteoclasts on bone slices were incubated twice with cold PBS for 15 min, followed by incubation with fresh α-10 medium containing 100 ng/ml RANKL, in the absence or presence 1 μM rotenone, 2 μg/ml antimycin A, or 2 μg/ml oligomycin for 5 hours. Then cells were fixed and stained with FITC-phalloidin.

G-actin/F-actin isolation

G-actin and F-actin were isolated using a commercial kit (Cytoskeleton Inc.). After 6 days of generation on bone particles, osteoclasts were starved with 2% α-MEM for 2h, followed by exposure to 100ng/mL M-CSF for 5min. Cells were lysed with F-actin stabilization buffer. 2mg of total lysate protein was used to separate soluble (G-actin) and insoluble (F-

actin) fractions by ultracentrifugation at 50,000 rpm/min for 1h at 37°C. The supernatant was designated as soluble G-actin and the pellet as insoluble F-actin and resolved with depolymerization buffer on ice for 2h. The samples were then analyzed by SDS-PAGE and western blot and densitometry.

Mito-Tracker staining and ATP quantification assay

Day 5 osteoclasts were incubated with pre-warmed staining solution containing 100 nM Mito-Tracker for 30 minutes. Then the cells were observed using a fluorescence microscope. ATP was quantified using an ATP Determination Kit (Invitrogen, A22066). Briefly, reaction mixture was added to the 96-well cell culture plate (100 μl/well) which contains the cultured cells or standard solution. After 30 min of incubation in dark, the plate was read using a luminescence detector. ATP concentrations were calculated using the standard curve.

XF Cell Mito Stress (Seahorse) analysis

Oxygen consumption rate (OCR) and extracellular acidification rate (ECAR) were measured using a Seahorse XFe96 Extracellular Flux Analyzer. BMMs were seeded in a Seahorse 96-well cell culture microplate at a density of 6 × 104 cells/well. The cells were osteoclast-induced with 100 ng/ml GST-RANKL and 30 ng/ml M-CSF for 6 days. On the day of the assay, culture media was changed to unbuffered DMEM (pH7.4) supplemented with 2.5 mM glucose, 200 ng/ml GST-RANKL and 100 ng/ml M-CSF. The cells were equilibrated for 1 h at 37 °C in a CO2-free incubator. The OCR measurement cycle consisted of 1.5-min mixing and 5-min measurement of the oxygen level. Testing of mitochondrial function was initiated by three baseline OCR measurement cycles. These were followed by the sequential injection of oligomycin (1 μM final concentration), FCCP (2 μM), and a mixture of rotenone (1 μM) and antimycin A (1 μM) with one OCR measurement cycle in between each injection and two final measurement cycles. OCR was calculated by the Seahorse XFe96 software, Wave. Based on the OCR measurements mitochondrial respiration parameters were calculated as follows: basal respiration, non-mitochondrial respiration (minimum measurement after rotenone/antimycin injection) was subtracted from the last measurement obtained before oligomycin injection; maximal respiration, measurement obtained after FCCP injection; oxygen consumption associated with ATP-coupled respiration, measurement after oligomycin injection was subtracted from the last measurement before oligomycin injection; spare respiratory capacity, basal respiration subtracted from maximal respiration. For the measurement of ECAR, culture media was changed to basal DMEM without glucose, 200 ng/ml GST-RANKL and 100 ng/ml M-CSF. The cells were equilibrated for 1 h at 37 °C in a CO_2-free incubator. The ECAR measurement cycle consisted of 1.5-min mixing and 5-min measurement of the extracellular acidification. Testing of glycolysis was initiated by three baseline ECAR measurement cycles. These were followed by the sequential injection of glucose (100 mM final concentration), oligomycin (1 μM), and 2-DG (500 mM) one ECAR measurement cycle in between each injection and two final measurement cycles. ECAR was calculated by the Seahorse XFe96 software, Wave.

GTP-Rac1 detection assay

The GTP-Rac1 was detected using Active Rac1 Pull-Down and Detection Kit (Thermo Fisher Scientific). Briefly, day 3 pre-osteoclasts were starved for 3 h in α-MEM medium

containing 2% FBS, lifted with 0.01% EDTA. Then the cells were seeded on the vitronectin-coated petri-dish or leaved in 50 ml conical tubes in suspension at 37°C for 30 min. Cells were lysed with Lysis/Binding/Wash Buffer. After quantification of the protein concentration, 500 μg cell lysates together with 20μg GST-human Pak1-PBD were added to the pretreated glutathione resin for incubation at 4°C for 1 hour. Then the resin was washed 3 times, and protein was eluted using 2×reducing sample buffer for the following western blotting.

Electron microscope for mitochondrial morphology

Tibias of 3-month-old mice were fixed with 5% glutaraldehyde in 0.16M collidine buffer (pH 7.4) overnight, followed by decalcified in 5% EDTA/0.1% glutaraldehyde for 5 days. Then the samples were fixed in 2% OsO4/3% K-ferrocyanide for 2 h, dehydrated in ethanol, and embedded in Epon LX 112. Sections were examined using a JEOL 100SX transmission electron microscope (JEOL USA, Peabody, MA, USA).

Statistics

Statistical significance was determined using Student's t test or 2 way ANOVA test. Data are expressed as mean ± SD. *$p < 0.05$, **$p < 0.01$, and ***$p < 0.001$ in all experiments.

Supplementary Material

Refer to Web version on PubMed Central for supplementary material.

Acknowledgments

This work was supported by Shriners Hospitals for Children grant 85400-STL (SLT); National Institutes of Health grants R37 AR046523 (SLT), R01 DK111389 (SLT), P30 AR057235 (SLT and DJV), R01 AR070030 (DJV), R01 DK11003402 (JS), and P30 DK020579 (JS). Authors' roles: Study design: all authors. Study conduct: YZ. Data collection: YZ. Data analysis: all authors. Data interpretation: all authors. Drafting manuscript: WZ and SLT. Approving final version of manuscript: WZ and SLT. WZ and SLT take responsibility for the integrity of the data analysis.

References

1. Novack DV, Teitelbaum SL. The osteoclast: friend or foe? Annu Rev Pathol. 2008; 3:457–84. Epub 2007/11/28. [PubMed: 18039135]
2. Zhao H, Ito Y, Chappel J, Andrews NW, Teitelbaum SL, Ross FP. Synaptotagmin VII regulates bone remodeling by modulating osteoclast and osteoblast secretion. Dev Cell. 2008; 14(6):914–25. Epub 2008/06/10. [PubMed: 18539119]
3. Ishii KA, Fumoto T, Iwai K, Takeshita S, Ito M, Shimohata N, et al. Coordination of PGC-1beta and iron uptake in mitochondrial biogenesis and osteoclast activation. Nat Med. 2009; 15(3):259–66. Epub 2009/03/03. [PubMed: 19252502]
4. Wei W, Wang X, Yang M, Smith LC, Dechow PC, Sonoda J, et al. PGC1beta mediates PPARgamma activation of osteoclastogenesis and rosiglitazone-induced bone loss. Cell Metab. 2010; 11(6):503–16. Epub 2010/06/04. [PubMed: 20519122]
5. Izawa T, Rohatgi N, Fukunaga T, Wang QT, Silva MJ, Gardner MJ, et al. ASXL2 Regulates Glucose, Lipid, and Skeletal Homeostasis. Cell reports. 2015; 11(10):1625–37. Epub 2015/06/09. [PubMed: 26051940]
6. Chabadel A, Banon-Rodriguez I, Cluet D, Rudkin BB, Wehrle-Haller B, Genot E, et al. CD44 and beta3 integrin organize two functionally distinct actin-based domains in osteoclasts. Mol Biol Cell. 2007; 18(12):4899–910. Epub 2007/09/28. [PubMed: 17898081]

7. Zou W, Kitaura H, Reeve J, Long F, Tybulewicz VL, Shattil SJ, et al. Syk, c-Src, the alphavbeta3 integrin, and ITAM immunoreceptors, in concert, regulate osteoclastic bone resorption. J Cell Biol. 2007; 176(6):877–88. Epub 2007/03/14. [PubMed: 17353363]
8. Zou W, Izawa T, Zhu T, Chappel J, Otero K, Monkley SJ, et al. Talin1 and Rap1 are critical for osteoclast function. Mol Cell Biol. 2013; 33(4):830–44. Epub 2012/12/12. [PubMed: 23230271]
9. Izawa T, Zou W, Chappel JC, Ashley JW, Feng X, Teitelbaum SL. c-Src links a RANK/alphavbeta3 integrin complex to the osteoclast cytoskeleton. Mol Cell Biol. 2012; 32(14):2943–53. Epub 2012/05/23. [PubMed: 22615494]
10. Zou W, Teitelbaum SL. Absence of Dap12 and the alphavbeta3 integrin causes severe osteopetrosis. J Cell Biol. 2015; 208(1):125–36. Epub 2014/12/31. [PubMed: 25547154]
11. Gomes LC, Di Benedetto G, Scorrano L. During autophagy mitochondria elongate, are spared from degradation and sustain cell viability. Nat Cell Biol. 2011; 13(5):589–98. Epub 2011/04/12. [PubMed: 21478857]
12. Zou W, Deselm CJ, Broekelmann TJ, Mecham RP, Vande Pol S, Choi K, et al. Paxillin contracts the osteoclast cytoskeleton. J Bone Miner Res. 2012; 27(12):2490–500. Epub 2012/07/19. [PubMed: 22807029]
13. Nayal A, Webb DJ, Brown CM, Schaefer EM, Vicente-Manzanares M, Horwitz AR. Paxillin phosphorylation at Ser273 localizes a GIT1-PIX-PAK complex and regulates adhesion and protrusion dynamics. J Cell Biol. 2006; 173(4):587–9. Epub 2006/05/24. [PubMed: 16717130]
14. Menon P, Yin G, Smolock EM, Zuscik MJ, Yan C, Berk BC. GPCR kinase 2 interacting protein 1 (GIT1) regulates osteoclast function and bone mass. J Cell Physiol. 2010; 225(3):777–85. Epub 2010/06/23. [PubMed: 20568227]
15. Pang J, Xu X, Getman MR, Shi X, Belmonte SL, Michaloski H, et al. G protein coupled receptor kinase 2 interacting protein 1 (GIT1) is a novel regulator of mitochondrial biogenesis in heart. J Mol Cell Cardiol. 2011; 51(5):769–76. Epub 2011/07/16. [PubMed: 21756914]
16. Takeshita S, Fumoto T, Matsuoka K, Park KA, Aburatani H, Kato S, et al. Osteoclast-secreted CTHRC1 in the coupling of bone resorption to formation. J Clin Invest. 2013; 123(9):3914–24. Epub 2013/08/03. [PubMed: 23908115]
17. Cusick T, Chen CM, Pennypacker BL, Pickarski M, Kimmel DB, Scott BB, et al. Odanacatib treatment increases hip bone mass and cortical thickness by preserving endocortical bone formation and stimulating periosteal bone formation in the ovariectomized adult rhesus monkey. J Bone Miner Res. 2012; 27(3):524–37. Epub 2011/11/25. [PubMed: 22113921]
18. Kuznetsov AV, Javadov S, Guzun R, Grimm M, Saks V. Cytoskeleton and regulation of mitochondrial function: the role of beta-tubulin II. Frontiers in physiology. 2013; 4:82. Epub 2013/05/01. [PubMed: 23630499]
19. Miyazaki T, Iwasawa M, Nakashima T, Mori S, Shigemoto K, Nakamura H, et al. Intracellular and extracellular ATP coordinately regulate the inverse correlation between osteoclast survival and bone resorption. J Biol Chem. 2012; 287(45):37808–23. Epub 2012/09/19. [PubMed: 22988253]
20. Indo Y, Takeshita S, Ishii KA, Hoshii T, Aburatani H, Hirao A, et al. Metabolic regulation of osteoclast differentiation and function. J Bone Miner Res. 2013; 28(11):2392–9. Epub 2013/05/11. [PubMed: 23661628]
21. Rodgers JT, Lerin C, Haas W, Gygi SP, Spiegelman BM, Puigserver P. Nutrient control of glucose homeostasis through a complex of PGC-1alpha and SIRT1. Nature. 2005; 434(7029):113–8. Epub 2005/03/04. [PubMed: 15744310]
22. Faccio R, Novack DV, Zallone A, Ross FP, Teitelbaum SL. Dynamic changes in the osteoclast cytoskeleton in response to growth factors and cell attachment are controlled by beta3 integrin. J Cell Biol. 2003; 162(3):499–509. Epub 2003/08/06. [PubMed: 12900398]

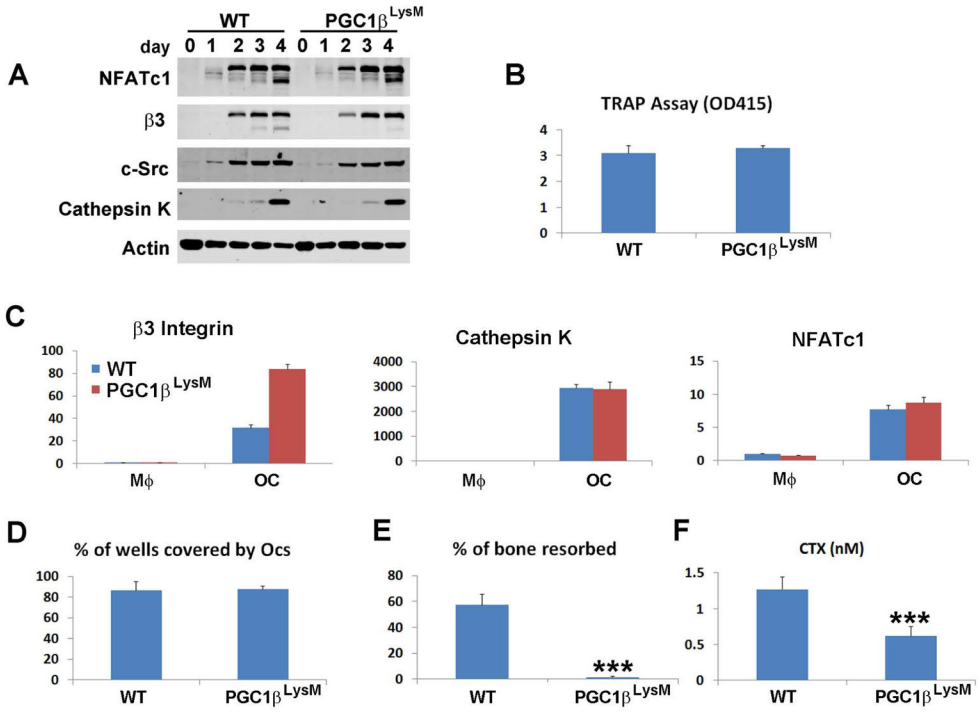

Figure 1. PGC1β deficiency impairs osteoclast function but not differentiation

A) WT and PGC1β^{LysM} BMMs were cultured with M-CSF and RANKL for as indicated days and differentiation markers determined by immunoblot. B) WT and PGC1β^{LysM} BMMs were cultured with M-CSF and RANKL for 5 days. Cells were lysed and medium TRAP activity was determined. C) WT and PGC1β^{LysM} BMMs were cultured with M-CSF and RANKL (OC) or only M-CSF (Mϕ) for 5 days. mRNA of osteoclast differentiation markers was determined by qPCR D) WT and PGC1β^{LysM} BMMs were cultured with M-CSF and RANKL for 5 days. The cells were stained for TRAP activity and the % of well covered by osteoclasts was histomorphometrically determined E) WT and PGC1β^{LysM} BMMs were cultured on bone slices with M-CSF and RANKL for 6 days. The cells were removed the bone stained with peroxidase-conjugated wheat germ agglutinin. The percentage of bone surface exhibiting resorption pits was determined. F) WT and PGC1β^{LysM} BMMs were cultured on bone with M-CSF and RANKL for 6 days. Medium CTx was determined.

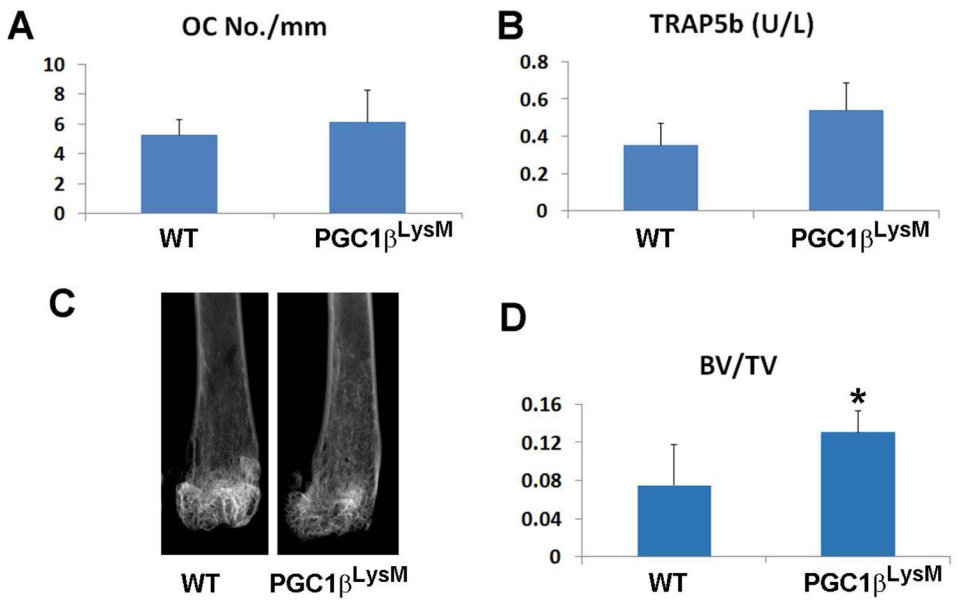

Figure 2. PGC1β^{LysM} mice have increased bone mass

A) Sections of femurs of 12 wk old WT (n=5) and PGC1β^{LysM} littermates (n=5) were TRAP stained. Osteoclast number/mm trabecular bone surface was determined. B) 12 wk old WT (n=5) and PGC1β^{LysM} littermates (n=5) were starved overnight and serum TRAP5b was determined. C) X-ray of femurs of 12 wk old WT and PGC1β^{LysM} littermates. D) Femurs of 12 wk old female WT (n=5) and PGC1β^{LysM} littermates (n=5) were subjected to μCT analysis.

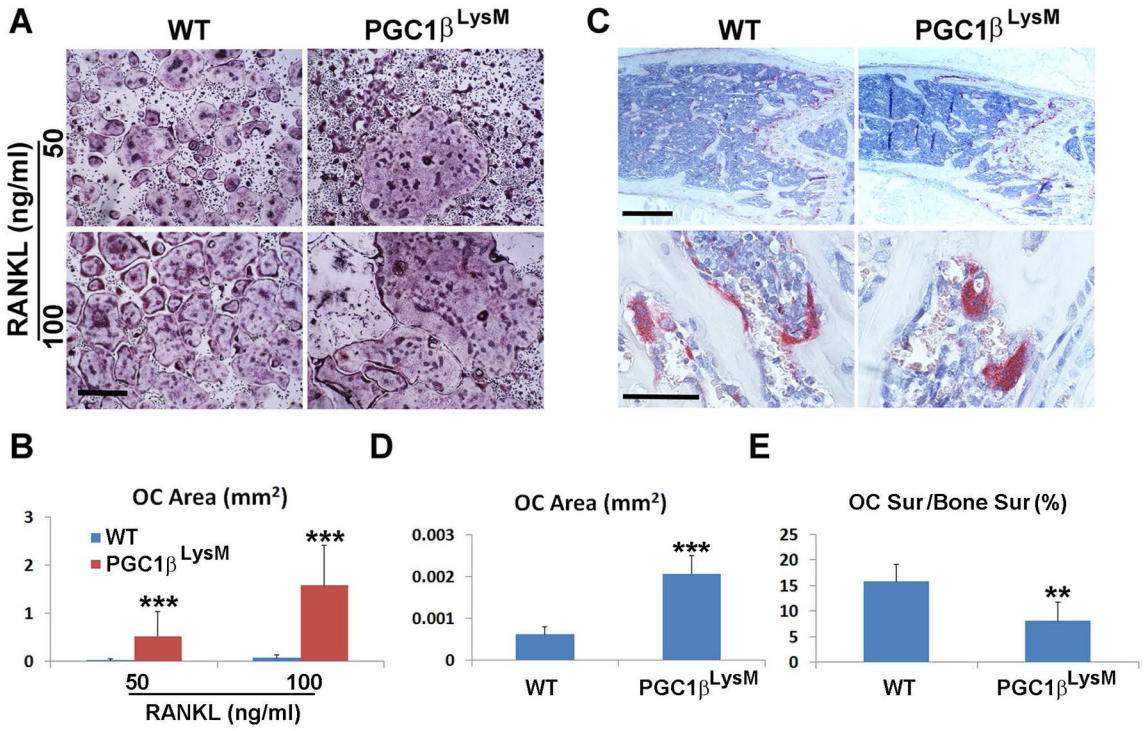

Figure 3. PGC1β^{LysM} osteoclasts are enlarged

A) WT and PGC1β^{LysM} BMMs were cultured with M-CSF and RANKL for 5 days and stained for TRAP activity. Scale bar: 500 μm. B) Size (area) of cultured WT and PGC1β^{LysM} osteoclasts. C) Sections of femurs of 12 wk old WT and PGC1β^{LysM} littermates stained for TRAP activity. Scale bar: upper panel 500 μm; lower panel 50 μm. D) Size (area) of WT and PGC1β^{LysM} osteoclasts in vivo. E) % of osteoclast surface juxtaposed to bone in femurs of 12 wk old WT (n=5) and PGC1β^{LysM} littermates (n=5).

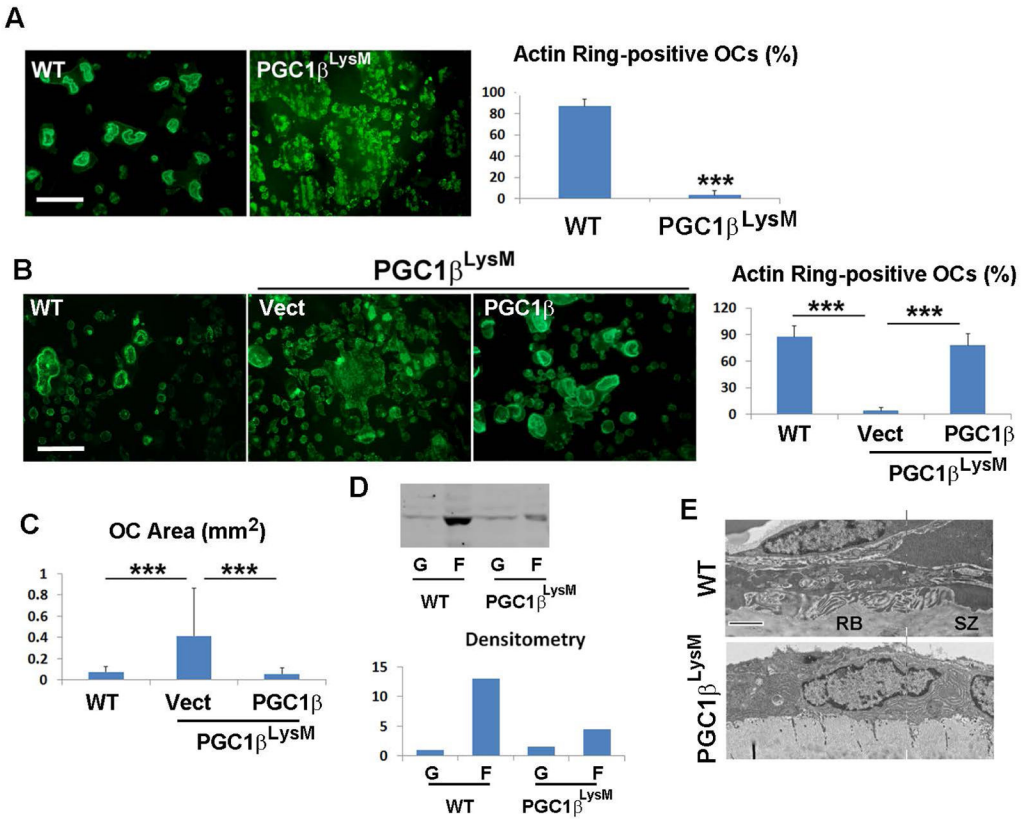

Figure 4. PGC1β organizes the osteoclast cytoskeleton

A) WT and PGC1β^{LysM} BMMs were cultured on bone slices with M-CSF and RANKL for 6 days and stained with FITC-phalloidin. The % of osteoclasts exhibiting actin rings was determined. Scale bar: 100 μm. B) WT and PGC1β^{LysM} BMMs, transduced with PGC1β or vector, were exposed to M-CSF and RANKL for 6 days and stained with FITC-phalloidin. The % of osteoclasts exhibiting actin rings was determined. Scale bar: 100 μm. C) WT and PGC1β^{LysM} BMMs, transduced with PGC1β or vector, were exposed to M-CSF and RANKL for 5 days. Osteoclast size (area) histomorphometrically determined. D) (Upper) Immunoblot of G-actin and F-actin in 2 mg of protein derived from WT and PGC1β^{LysM} bone-residing osteoclasts. (Bottom) Densitometric analysis of immunoblot. E) Ultrastructure of osteoclasts in femurs of 12 wk old WT and PGC1β^{LysM} littermates. (RB, ruffled border; SZ, sealing zone). Scale bar: 2 μm.

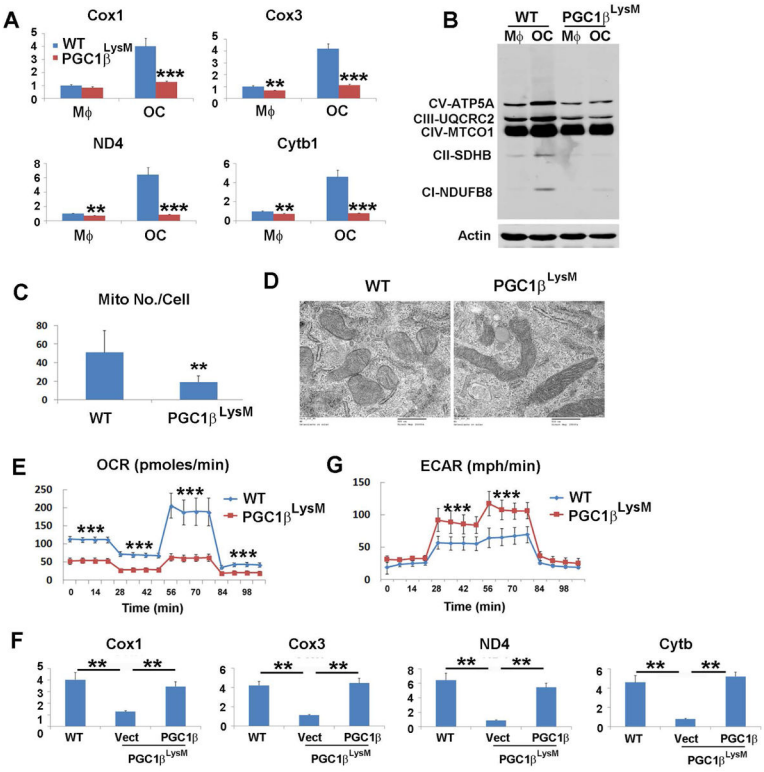

Figure 5. Mitochondrial abundance and function are decreased in PGC1β^{LysM} osteoclasts

A) WT and PGC1β^{LysM} BMMs were cultured with M-CSF +/− RANKL for 5 days. Abundance of mitochondrial biogenesis markers mRNA was determined by qPCR in macrophages and osteoclasts. B) WT and PGC1β^{LysM} BMMs were cultured with M-CSF +/− RANKL for 5 days. OXPHOS complex abundance was determined by immunoblot in macrophages and osteoclasts. C) WT and PGC1β^{LysM} BMMs cultured with M-CSF and RANKL for 5 days were subjected to electronic microscopic analysis. Mitochondria number/cell was determined. D) Ultrastructural appearance of mitochondria of WT and PGC1β^{LysM} osteoclasts generated in vitro by 5 days exposure to M-CSF and RANKL. Scale bar: 500 nm. E) WT and PGC1β^{LysM} BMMs were cultured with M-CSF and RANKL for 5 days. Oxygen consumption rate (OCR) and glycolysis (ECAR) were analyzed by XF Cell Mito Stress Assay. F) WT and PGC1β^{LysM} BMMs, transduced with PGC1β or vector, were exposed to M-CSF and RANKL for 5 days. Abundance of mitochondrial biogenesis marker mRNA was determined by qPCR. G) WT and PGC1β^{LysM} BMMs were cultured with M-CSF and RANKL for 5 days. Extracellular acidification rate (ECAR) was analyzed by XF Cell Glycolysis Assay, followed by sequential injection of glucose (100 mM final concentration), oligomycin (1 μM), and 2-DG (500 mM).

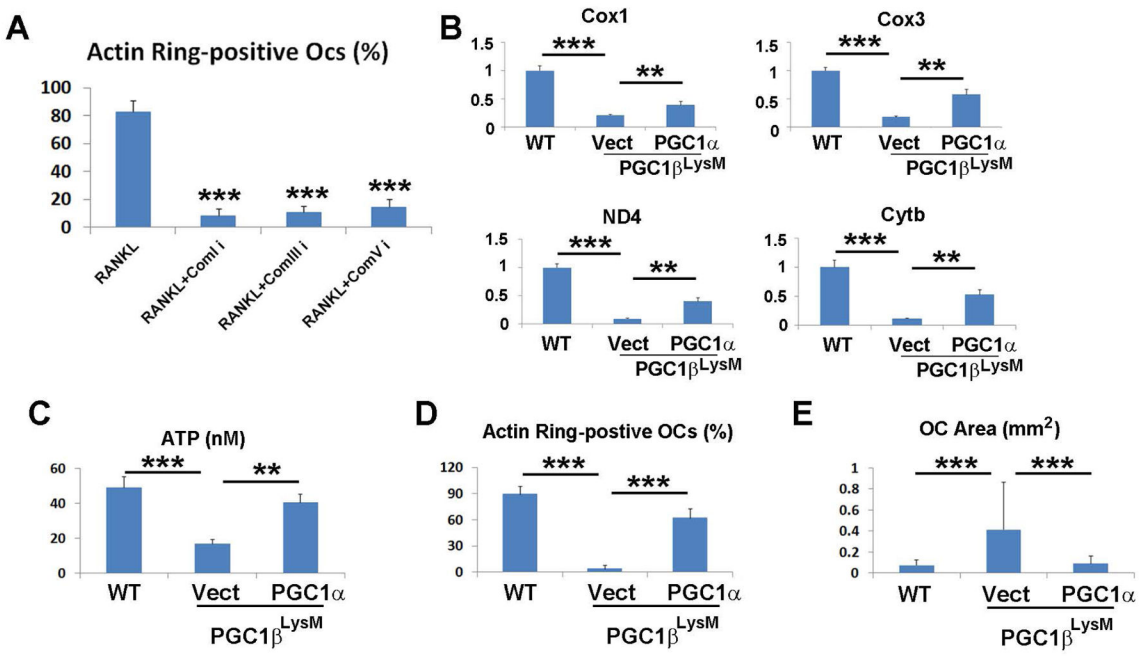

Figure 6. Mitochondrial OXPHOS regulates the osteoclast cytoskeleton

A) WT osteoclasts on bone slices were washed with cold PBS. RANKL was added alone or with mitochondrial complex specific inhibitors for 5h. The cells were stained with FITC-phalloidin and the % exhibiting actin rings determined. Scale bar: 100 μm. B) WT and PGC1β^{LysM} BMMs, transduced with PGC1α or vector, were exposed to M-CSF and RANKL for 5 days. Abundance of mitochondrial biogenesis markers mRNA was determined by qPCR. C) WT and PGC1β^{LysM} BMMs, transduced with PGC1α or vector, were exposed to M-CSF and RANKL for 5 days and ATP – coupled respiration determined. D) WT and PGC1β^{LysM} BMMs, transduced with PGC1α or vector, were exposed to M-CSF and RANKL for 6 days. The cells were stained with FITC-phalloidin and the % forming actin rings was quantified. E) WT and PGC1β^{LysM} BMMs, transduced with PGC1α or vector, were exposed to M-CSF and RANKL for 5 days and stained for TRAP activity. Osteoclast size (area) was histomorphometrically determined.

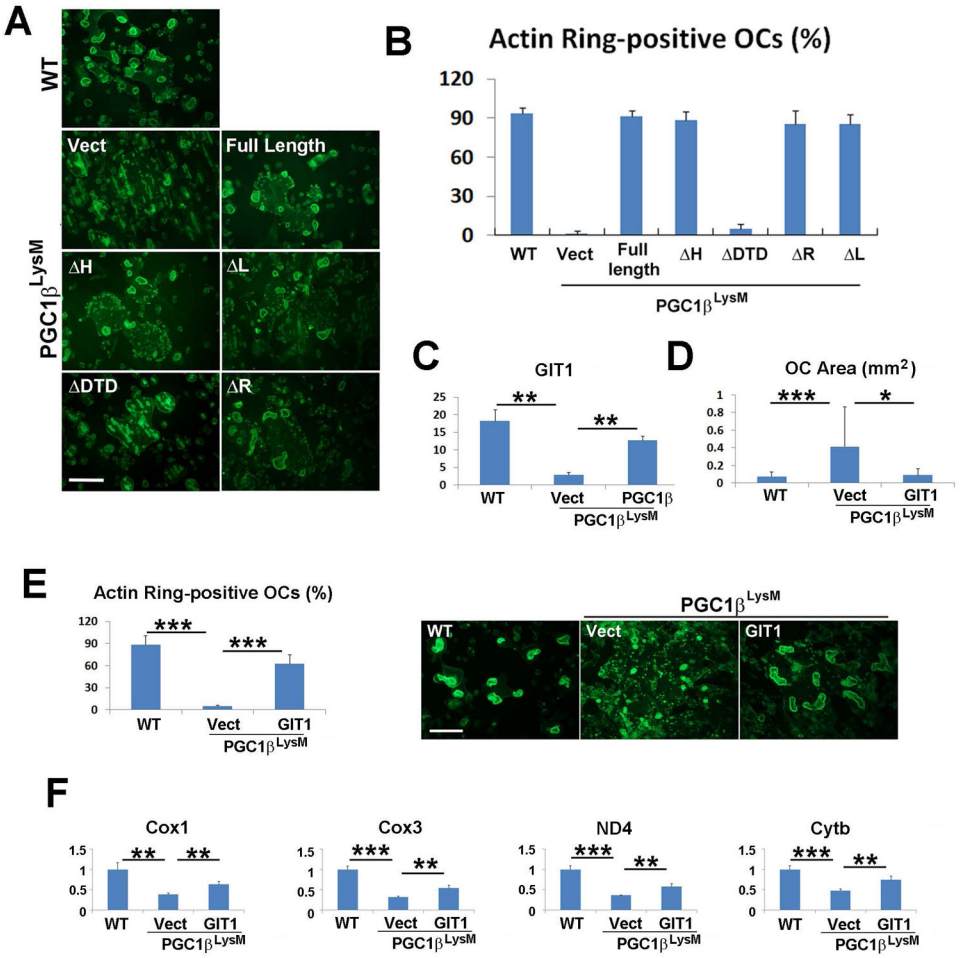

Figure 7. GIT1 mediates PGC1β-induced osteoclast cytoskeleton organization

A and B) WT and PGC1β^{LysM} BMMs, transduced with vector, PGC1β, or various PGC1β deletion mutants were exposed to M-CSF and RANKL on bone for 6 days. A) Actin rings were stained with FITC-phalloidin. Scale bar: 100 μm. B) the % exhibiting actin rings determined. C) WT and PGC1β^{LysM} BMMs, transduced with PGC1β or vector, were exposed to M-CSF and RANKL for 5 days. GIT1 mRNA was determined by qPCR. D) WT and PGC1β^{LysM} BMMs, transduced with GIT1 or vector, were exposed to M-CSF and RANKL for 5 days. Cells were stained for TRAP activity and their size (area) histomorphometrically determined. E) WT and PGC1β^{LysM} BMMs, transduced with GIT1 or vector, were exposed to M-CSF and RANKL on bone for 6 days. The cells were stained with FITC-phalloidin and the % forming actin rings was quantified. F) WT and PGC1β^{LysM} BMMs, transduced with GIT1 or vector, were exposed to M-CSF and RANKL for 5 days. Abundance of mitochondrial biogenesis markers mRNA was determined by qPCR.